Hindawi Publishing Corporation
Journal of Applied Mathematics
Volume 2012, Article ID 758657, 31 pages
doi:10.1155/2012/758657

Research Article

Analysis of Edge Detection in Bar Code Symbols: An Overview and Open Problems

Saša Krešić-Jurić

Faculty of Mathematical and Natural Sciences, University of Split, Teslina 12, 21000 Split, Croatia

Correspondence should be addressed to Saša Krešić-Jurić, skresic@pmfst.hr

Received 1 May 2012; Revised 29 July 2012; Accepted 31 July 2012

Academic Editor: Carlos J. S. Alves

Accurate edge localization is essential in bar code decoding. Since speckle noise is the most dominant form of noise in laser bar code scanners, it is important to fully understand its effects on edge detection. Starting with the basic statistical properties of speckle patterns, we present stochastic analysis of speckle noise. We derive the autocorrelation function and power spectral density (PSD) of the noise in terms of intensity distribution of the scanning beam. We then study the signal-to-noise ratio for signals that result from scanning different configurations of edges. Next, we consider statistical properties of edge localization error caused by speckle noise. We show that the standard deviation of the error is determined by the PSD of the noise and relative positions of edges in a bar code symbol. Based on the analysis presented here, we propose new criteria for system design.

1. Introduction

Image processing, traditionally an engineering field, has recently attracted attention of the mathematical community. One of the most important image features is edges which are modeled as discontinuities in the gray level of an image. Edge detection is concerned with localization of these discontinuities. Information extracted from edges is used for image processing such as segmentation, recognition, enhancement, and compression. Edge detection also finds an important application in laser bar code scanning. Information stored in a linear bar code is encoded in a string $\mathcal{S} = (p_1, p_2, \ldots, p_n)$, called digital bar pattern, which represents a sequence of widths of black bars and white spaces. The way information is stored in a bar code symbol depends on the symbology [1]. One of the most popular symbologies is the universal product code version A (UPCA) which is widely used in retail stores. Figure 1 shows a UPCA symbol encoding the digits "0122345678905." UPCA symbols encode twelve digits where each digit consists of two bars and two spaces (code words) with a total width

Table 1: UPCA encodation patterns.

Number	Pattern
0	(3, 2, 1, 1)
1	(2, 2, 2, 1)
2	(2, 1, 2, 2)
3	(1, 4, 1, 1)
4	(1, 1, 3, 2)
5	(1, 2, 3, 1)
6	(1, 1, 1, 4)
7	(1, 3, 1, 2)
8	(1, 2, 1, 3)
9	(3, 1, 1, 2)

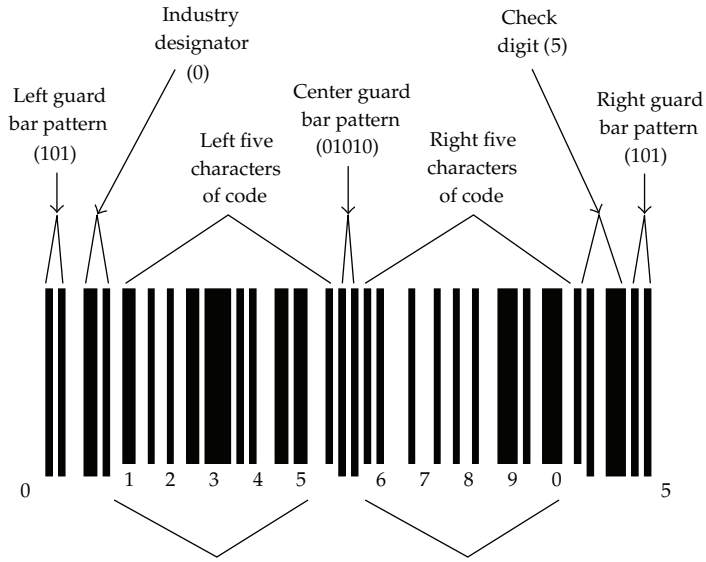

Figure 1: UPCA bar code encoding the digits "012345678905."

of seven modules. Encodation patterns for digits between 0 and 9 are listed in Table 1 in Section 4.2. For decoding purposes, it is important to keep track of the scanning direction. Thus, each digit is assigned two code words which are mirror images of each other: those on the right side of the symbol start with a bar and those used on the left side start with a space. Each UPCA symbol contains the following groups of code words (see Figure 1):

(1) a left guard pattern 101,

(2) six digits on the left side: one digit denoting industry type and five digits with manufacturer's code,

(3) a center guard pattern 01010,

(4) six digits on the right side: five digits with item code and one check digit,

(5) a right guard pattern 101.

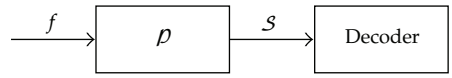

Figure 2: Bar code signal processing diagram. Signal processor $\mathcal{D}$ produces digital bar pattern $\mathcal{S}$.

The structure of the UPCA symbols allows "scanning by halves" since each half can be scanned separately, and the symbol can be put together afterwards. This gives the advantage of scanning UPCA bar code from different directions. Since the resulting digital bar pattern is recovered from the positions of bar/space edges, accurate edge localization is critical in bar code decoding.

Bar code signal processing can be viewed as an input-output system schematically shown in Figure 2. Here, $f(t)$ is an observed signal (photodetector current in a laser scanner), and $\mathcal{D}$ represents a signal processor. The processor $\mathcal{D}$ depends on signal modeling and representation. If the signal derivative $f'(t)$ is modeled as a hidden Markov chain, then $\mathcal{D}$ is based on maximum likelihood estimation [2]. The digital bar pattern is chosen such that it fits the observed data $f'(t)$ with the highest probability. The statistical properties of $f'(t)$ can be modeled from heuristic considerations or inferred using learning theory such as the Baum-Welch algorithm [3]. A bar code signal $f(t)$ can also be modeled as a function of bounded variation. In this case, the signal processor is based on minimization of a total variation functional over an appropriate function space [4]. The minimization algorithm performs both filtering and deblurring, and it is very robust under high noise and blur. However, it is computationally expensive for implementation in commercial scanners. For related total variation-based techniques in image processing, see [5–9]. Edge detection techniques based on multiresolution analysis, anisotropic diffusion filtering, and level set methods can be found in [10–18].

In this paper, we consider edge detection in bar code symbols based on Canny's algorithm [19, 20]. It relies on finding local extrema of $f'(t)$ where $f(t)$ is assumed to be a C^2 function. Here, the signal processor $\mathcal{D}$ consists of three steps: differentiation, filtering, and edge labeling. The signal is filtered in order to regularize the derivative operator which amplifies high frequencies. Edge labelling is a process in which true edges are separated from noised or false edges. When the edges are labelled, a digital bar pattern is produced and sent to a decoder for further processing.

Laser bar code scanners are very sensitive to noise because an error in the position of a single edge may cause a failure to read the bar code or to read it incorrectly. There are several sources of noise in a bar code scanner: Johnson or thermal noise, shot noise, and speckle noise. Thermal and shot noise are noise currents that are observed in electronic circuits [21, 22]. Thermal noise [23, 24] is associated with random fluctuations of the velocities of electrons in a conductor. It is independent of any applied voltage, and hence, it is present even if no current flows in the conductor. Shot noise [25] is generated by fluctuations of the number of electrons, and it manifests itself only when a current flows in a conductor. The power spectral densities of both types of noise are nearly constant throughout the frequency spectrum. The power of thermal noise is given by the Nyquist formula

$$P_{\text{thermal}} = 4k_B T \Delta f, \tag{1.1}$$

where k_B is the Boltzmann's constant, T is the temperature in Kelvins, and Δf is the frequency band. Similarly, the power of shot noise is

$$P_{\text{shot}} = 2eIR\Delta f, \tag{1.2}$$

where e is the electron charge, I is the current, and R is the resistance of the conductor. The power of thermal noise in a scanner is normally several times greater than the power of shot noise. A more recent review of the properties of thermal and shot noise can be found in [26, 27].

In contrast to thermal and shot noise, speckle noise is an optical phenomenon which results when spatially coherent electromagnetic (EM) field is scattered from a diffuse surface, such as paper on which a bar code is printed. The scattered light forms a random interference pattern in the photodetector aperture. As the laser beam moves across the surface, temporal changes in the intensity of the pattern induce fluctuations in the photodetector current. It turns out that under normal operating conditions the effects of thermal and shot noise are negligible compared to speckle noise, which is the main factor limiting the performance of a bar code scanner. Only in long-range applications, when the photodetector signal is weak, the performance is limited by a mixture of electronic and speckle noise. Therefore, in this work, we limit our attention to speckle noise and investigate its effects on edge detection. We present stochastic properties of speckle noise and study the signal-to-noise ratio and edge localization error caused by the noise. We remark that speckle noise is difficult to filter because its spectrum often overlaps with the spectrum of a noise-free signal. However, investigation of the effects of speckle noise on edge detection may lead to more efficient filtering techniques.

The paper is organized as follows. In Section 2, we give an overview of statistical properties of static speckle patterns. We then study dynamic speckle which induces noise in the photodetector signal. We show that speckle noise is a weakly stationary random process and calculate the autocorrelation function and power spectral density of the noise. Since differentiation is used in edge detection, we also study stochastic properties of differentiated speckle noise. Section 3 is devoted to estimating the signal-to-noise ratio for bar code signals corrupted by speckle noise. As a toy model, we study signals obtained by scanning a single edge and an infinite sequence of edges. In Section 4, we address the problem of finding the edge localization error. We derive a first-order approximation of the error in terms of the power spectral density of speckle noise. We show that the standard deviation of the error depends on spectral characteristics of the noise and on relative locations of edges in a bar code symbol. This result is used to study susceptibility of different bar code symbols to edge localization error. Finally, we discuss how the theoretical analysis presented here can be used in system design. In particular, we propose a new criterion for estimating the working range of a scanner based on the combined effect of convolution distortion and edge localization error.

2. Statistical Properties of Speckle Noise

2.1. Statistics of Speckle Patterns

This section summarizes the basic properties of speckle relevant to applications in bar code scanning. Consider the free space propagation geometry shown in Figure 3. A focused laser beam is incident on a diffuse surface, and the scattered wave is captured by a photodetector

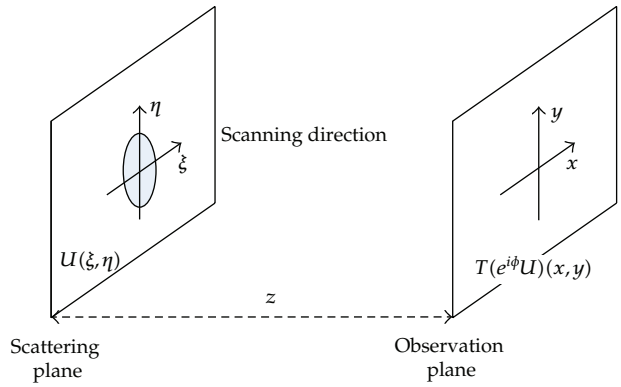

Figure 3: Free-space propagation model of scattered light. $U(\xi, \eta)$ is the incident optical field in the scattering plane, and $T(e^{i\phi}U)\ (x, y)$ is the optical field of the interference pattern in the observation plane.

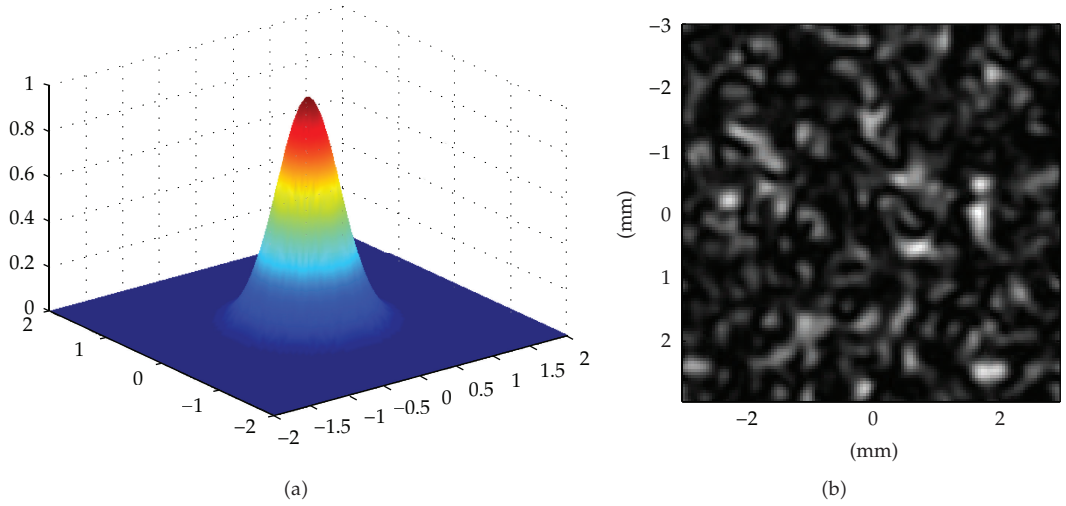

Figure 4: (a) Gaussian beam with optical field $U(\xi, \eta) = U_0 \exp[-(\xi/\omega)^2 - (\eta/\omega)^2]$ and beam radius ω. (b) Speckle pattern in the photodetector plane generated by a Gaussian beam.

in the observation plane. A speckle pattern formed in the observation plane results from interference of EM waves reflected from a large number of microscopic scatterers randomly distributed in the illuminated region. The pattern is characterized by a multitude of tiny spots (speckle) of varying size and intensity. Figure 4 shows a Gaussian beam incident on the scattering surface and the resulting speckle pattern. A comprehensive review of speckle properties can be found in Goodman's chapter in [28]. More recent developments in the field have been discussed in [29, 30].

In our analysis, we assume the same conventional model of the scattering surface as in [28]. Let $U \in L^2(\mathbb{R}^2)$ be a complex-valued function which describes the scalar components of the EM field of the laser beam. A description of only one component is sufficient to describe

the properties of the beam. The scattered waves are randomly dephased; hence, the EM field transforms according to

$$U(\xi,\eta) \longmapsto e^{i\phi(\xi,\eta)}U(\xi,\eta), \tag{2.1}$$

where $\phi(\xi,\eta)$ is a random phase acquired at the point (ξ,η) in the scattering plane. We make the following assumptions about the random function $\phi(\xi,\eta)$:

(i) the phase $\phi(\xi,\eta)$ is uniformly distributed in $[-\pi,\pi]$ at each point $(\xi,\eta) \in \mathbb{R}^2$,

(ii) $\phi(\xi_1,\eta_1)$ is uncorrelated with $\phi(\xi_2,\eta_2)$ for all $(\xi_1,\eta_1) \neq (\xi_2,\eta_2)$.

The EM field in the observation plane is given by the Fresnel integral transformation [31]

$$T\left(e^{i\phi}U\right)(x,y) = \int_{\mathbb{R}^2} e^{i\phi(\xi,\eta)}U(\xi,\eta)K(x-\xi,y-\eta)d\xi\,d\eta, \tag{2.2}$$

where K is the convolution kernel

$$K(x,y) = \frac{e^{ikz}}{i\lambda z}\exp\left[i\left(\frac{k}{2z}\left(x^2+y^2\right)\right)\right], \tag{2.3}$$

$k = 2\pi/\lambda$, λ is the optical wavelength, and z is the distance between the scattering and observation planes. The transformation $T : L^2(\mathbb{R}^2) \to L^2(\mathbb{R}^2)$ is a bounded operator with unit norm $\|T\| = \sup\{\|T(u)\| \mid u \in L^2(\mathbb{R}^2), \|u\| = 1\}$ where $\|\cdot\|$ denotes the L^2-norm on $\mathbb{R}^2$, $\|u\| = \left(\int_{\mathbb{R}^2} |u(x,y)|^2 dx\,dy\right)^{1/2}$. The intensity of a speckle pattern in the observation plane is given by

$$I_s(x,y) = \left|T\left(e^{i\phi}U\right)(x,y)\right|^2. \tag{2.4}$$

Assumptions (i) and (ii) imply that $I_s = \{I_s(x,y) \mid (x,y) \in \mathbb{R}^2\}$ is a weakly stationary random process. Hence, the expected value $\mathbf{E}[I_s(x,y)]$ is independent of the observation point. It is related to the physical characteristics of the system by

$$\mathbf{E}\left[I_s(x,y)\right] = \rho P\,\frac{\cos(\theta)}{\pi z^2}, \tag{2.5}$$

where $P = \|U\|^2$ is the power of the optical field, $\rho \in (0,1]$ is the reflectance of the scattering surface, and θ is the angle between the direction of specular reflection and direction of observation [32]. Let us denote $\mathbf{E}[I_s(x,y)] = \langle I_s \rangle$. The probability density function of $I_s(x,y)$ follows the negative exponential law [28]

$$p(I_s) = \frac{1}{\langle I_s \rangle}\exp\left(-\frac{I_s}{\langle I_s \rangle}\right), \tag{2.6}$$

and the variance is given by

$$\sigma_s^2 = \mathbf{E}\Big[\big(I_s(x,y) - \langle I_s\rangle\big)^2\Big] = \langle I_s\rangle^2. \tag{2.7}$$

Thus, the contrast $\sigma_s/\langle I_s\rangle$ of a speckle pattern is always unity.

Since the process I_s is weakly stationary, the autocorrelation function $R_s(x_1, y_1; x_2, y_2) = \mathbf{E}[I_s(x_1, y_1)I_s(x_2, y_2)]$ depends only on separation between the observation points (x_1, y_1) and (x_2, y_2). It can be shown that R_s is given by [28]

$$R_s(x_1, y_1; x_2, y_2) = \langle I_s\rangle^2\Big(1 + \big|\mu(x_2 - x_1, y_2 - y_1)\big|^2\Big), \tag{2.8}$$

where μ is the complex coherence function of the optical field U defined by

$$\mu(x,y) = \frac{1}{\|U\|^2}\int_{\mathbb{R}^2} |U(\xi,\eta)|^2 \exp\left(i\frac{2\pi}{\lambda z}(x\xi + y\eta)\right)d\xi\, d\eta. \tag{2.9}$$

The function μ is related to the average speckle size in the following way. Intuitively, if the correlation between intensity levels $I_s(x_1, y_1)$ and $I_s(x_2, y_2)$ is high, then the points (x_1, y_1) and (x_2, y_2) belong to the same speckle cell. For a fixed point (x_1, y_2), it is reasonable to define the speckle correlation area (average speckle size) as

$$S_c = \int_{\mathbb{R}^2} \rho\big(I_s(x_1, y_1), I_s(x_1 + x, y_1 + y)\big)dx\, dy, \tag{2.10}$$

where ρ is the correlation coefficient

$$\rho\big(I_s(x_1, y_1), I_s(x_2, y_1)\big) = \frac{\operatorname{cov}\big(I_s(x_1, y_1), I_s(x_2, y_2)\big)}{\sigma_s^2}. \tag{2.11}$$

Here, $\operatorname{cov}(X_1, X_2) = \mathbf{E}[X_1X_2] - \mathbf{E}[X_1]\mathbf{E}[X_2]$ is the covariance of the random variables X_1 and X_2. Using (2.7) and (2.8), we find

$$\rho\big(I_s(x_1, y_1), I_s(x_2, y_2)\big) = \big|\mu(x_2 - x_2, y_2 - y_1)\big|^2. \tag{2.12}$$

Hence, the speckle correlation area is given by

$$S_c = \int_{\mathbb{R}^2} \big|\mu(x,y)\big|^2 dx\, dy. \tag{2.13}$$

Since the complex coherence function is proportional to the Fourier transform of the beam intensity $I(\xi,\eta) = |U(\xi,\eta)|^2$, one can use the Parseval's identity to obtain

$$S_c = (\lambda z)^2 \frac{\int_{\mathbb{R}^2} I^2(\xi,\eta)d\xi\, d\eta}{\left(\int_{\mathbb{R}^2} I(\xi,\eta)d\xi\, d\eta\right)^2}. \tag{2.14}$$

2.2. Power Spectral Density of Speckle Noise

In the preceding subsection, we discussed statistical properties of static speckle patterns. Next, we consider time-varying speckle which arises when a laser beam scans a surface of constant reflectance (e.g., white paper), as shown in Figure 3. Early analysis of speckle noise in laser scanning systems and comparison of theoretical results with experiment were given in [33]. The scattered light is converted to an electrical signal $f(t)$ by a photodetector. Temporal changes in the speckle pattern intensity induce random fluctuations, called speckle noise, about the average value of $f(t)$. The signal is a continuous time random process $f = \{f(t) \mid t \in \mathbb{R}\}$ where

$$f(t) = \mathcal{R} \int_{\mathbb{R}^2} A(x,y) I_s(x,y,t) dx\, dy. \tag{2.15}$$

Here, $I_s(x,y,t)$ is the speckle intensity at instant t, $\mathcal{R}$ is optical-to-electrical signal conversion factor, and the function $0 < A(x,y) \leq 1$ characterizes the photodetector response. A description of statistical properties of dynamic speckle can be found in [30]. We assume that A has compact support bounded by the photodetector aperture. Since the surface reflectance is constant, the expected value of $I_s(x,y,t)$ is independent of both space and time coordinates, that is, $\mathbf{E}[I_s(x,y,t)] = \langle I_s \rangle$ where $\langle I_s \rangle$ is given by (2.5). It follows from (2.15) that the expected value of $f(t)$ is given by

$$\mathbf{E}\big[f(t)\big] = \mathcal{R} A_d \langle I_s \rangle, \tag{2.16}$$

where $A_d = \int_{\mathbb{R}^2} A(x,y) dx\, dy$. Let us denote $\langle f \rangle = \mathcal{R} A_d \langle I_s \rangle$. In view of (2.5), $\langle f \rangle$ can be expressed as

$$\langle f \rangle = \rho P \mathcal{R} \Omega_d, \tag{2.17}$$

where $\Omega_d = A_d \cos(\theta)/(\pi z^2)$ represents the fraction of the scattered power of the beam captured by the detector aperture.

Important statistical properties of f can be derived from the autocorrelation function $R_f(t_1,t_2) = \mathbf{E}[f(t_1)f(t_2)]$. In view of (2.15), we find

$$R_f(t_1,t_2) = \mathcal{R}^2 \int_{\mathbb{R}^4} A(x_1,y_1) A(x_2,y_2) R_{ds}(x_1,y_1,x_2,y_2,t_1,t_2) dx_1 dy_1 dx_2 dy_2, \tag{2.18}$$

where $R_{ds}(x_1,y_1,x_2,y_2,t_1,t_2) = \mathbf{E}[I_s(x_1,y_1,t_1) I_s(x_2,y_2,t_2)]$ is the autocorrelation of dynamic speckle. Without loss of generality, we assume that the optical field U moves in the ξ-direction. The function R_{ds} can be found by considering R_{ds} to be the cross-correlation function of two static speckle patterns at instants $t = t_1$ and $t = t_2$. Using this argument, one can express R_{ds} in terms of the complex coherence function μ_d of the moving optical field as

$$R_{ds}(x_1,y_1,x_2,y_2,t_1,t_2) = \langle I_s \rangle^2 \Big(1 + \big|\mu_d(x_2 - x_1, y_2 - y_1, t_2 - t_1)\big|^2\Big), \tag{2.19}$$

where

$$\mu_d(x,y,\tau) = \frac{1}{\|U\|^2}\int_{\mathbb{R}^2} U(\xi,\eta)U^*(\xi - V\tau,\eta)\exp\left(i\frac{2\pi}{\lambda z}(\xi x + \eta y)\right)d\xi\, d\eta, \tag{2.20}$$

and U^* denotes the complex conjugate of U. We note that for $\tau = 0$ we have $\mu_d(x,y,0) = \mu(x,y)$. Thus, $R_{ds} = R_s$ when the two speckle patterns overlap. The behaviour of the complex coherence function μ_d for different optical fields is described in [32]. Substituting (2.19) into (2.18), we obtain

$$R_f(t_1,t_2) = \mathcal{R}^2\langle I_s\rangle^2\int_{\mathbb{R}^4} A(x_1,y_1)A(x_2,y_2)\left(1+\left|\mu_d(x_2-x_1,y_2-y_1,t_2-t_1)\right|^2\right)dx_1dy_1dx_2dy_2. \tag{2.21}$$

Introducing the variables $x = x_2 - x_1$, $y = y_2 - y_1$, and $\tau = t_2 - t_1$, the above integral takes the form

$$R_f(\tau) = \langle f\rangle^2\left(1 + \frac{1}{A_d^2}\int_{\mathbb{R}^2} R_A(x,y)\left|\mu_d(x,y,\tau)\right|^2\right)dx\,dy, \tag{2.22}$$

where

$$R_A(x,y) = \int_{\mathbb{R}^2} A(x_1,y_1)A(x_1+x,y_1+y)dx_1dy_1, \tag{2.23}$$

is the autocorrelation of the weighting function A. In many cases of practical interest, the magnitude of $|\mu_d(x,y,\tau)|^2$ tends to zero very rapidly as $|x|$ and $|y|$ increase, that is,

$$\max_{\tau\in\mathbb{R}}\left|\mu_d(x,y,\tau)\right|^2 \ll 1 \quad \forall|x|,|y| > \delta, \tag{2.24}$$

where $\delta > 0$ is small compared to the size of a detector aperture. Then, the integral in (2.22) can be approximated by

$$\int_{\mathbb{R}^2} R_A(x,y)\left|\mu_d(x,y,\tau)\right|^2dx\,dy \approx R_A(0,0)\int_{\mathbb{R}^2}\left|\mu_d(x,y,\tau)\right|^2dx\,dy, \tag{2.25}$$

which largely simplifies the calculation of $R_f(\tau)$. Validity of this approximation is justified by the example in Section 2.4. Using the approximation (2.25), we obtain

$$R_f(\tau) = \langle f\rangle^2\left(1 + \frac{1}{A_e}\int_{\mathbb{R}^2}\left|\mu_d(x,y,\tau)\right|^2dx\,dy\right), \tag{2.26}$$

where

$$A_e = \frac{A_d}{R_A(0,0)} = \frac{\left(\int_{\mathbb{R}^2}A(x,y)dx\,dy\right)^2}{\int_{\mathbb{R}^2}A^2(x,y)dx\,dy}, \tag{2.27}$$

is the effective aperture area. We note that if $A(x,y)$ is the characteristic function of the aperture, then $A_e = A_d$, the physical area of the aperture.

The autocorrelation $R_f(\tau)$ can be conveniently expressed in terms of the intensity distribution $I(\xi,\eta) = |U(\xi,\eta)|^2$ of the laser beam. Using (2.20) and applying the Parseval's identity, we find

$$\int_{\mathbb{R}^2} |\mu_d(x,y,\tau)|^2 dx\,dy = \frac{(\lambda z)^2}{\|U\|^4} \int_{\mathbb{R}^2} |U(\xi,\eta)|^2 |U(\xi - V\tau,\eta)|^2 d\xi\,d\eta. \tag{2.28}$$

Hence, (2.26) becomes

$$R_f(\tau) = \langle f \rangle^2 \left(1 + \frac{(\lambda z)^2}{A_e} \frac{\int_{\mathbb{R}^2} I(\xi,\eta) I(\xi - V\tau,\eta) d\xi\,d\eta}{\left(\int_{\mathbb{R}^2} I(\xi,\eta) d\xi, d\eta\right)^2}\right). \tag{2.29}$$

Therefore, the autocorrelation function of the signal $f(t)$ is completely determined by the intensity distribution of the scanning beam. A more intuitive expression for $R_f(\tau)$ is provided by substituting the speckle correlation area (2.14) into (2.29),

$$R_f(\tau) = \langle f \rangle^2 \left(1 + \frac{S_c}{A_e} \frac{1}{\|I\|^2} \int_{\mathbb{R}^2} I(\xi,\eta) I(\xi - V\tau,\eta) d\xi\,d\eta\right). \tag{2.30}$$

Note that the ratio A_e/S_c represents the average number of speckle correlation cells in the photodetector aperture (speckle density).

One can readily show that if the initial speckle pattern is a superposition of N statistically independent patterns, $I(x,y,t) = \sum_{k=1}^{N} I_k(x,y,t)$, with expected value $\mathbf{E}[I_k(x,y,t)] = \langle I_s \rangle / N$, then $R_f(\tau)$ is modified according to

$$R_f(\tau) = \langle f \rangle^2 \left(1 + \frac{S_c}{N A_e} \frac{1}{\|I\|^2} \int_{\mathbb{R}^2} I(\xi,\eta) I(\xi - V\tau,\eta) d\xi\,d\eta\right). \tag{2.31}$$

This observation is important because when a polarized laser beam is scattered from a dielectric surface, it gets depolarized. The resulting speckle pattern is then equivalent to a superposition of $N = 2$ independent patterns.

Since $\mathbf{E}[f(t)]$ and $R_f(t_1,t_2)$ are invariant under time translation, the process f is weakly stationary. By the Wiener–Khinchin theorem [34, 35], the power spectral density (PSD) of f is the Fourier transform of the autocorrelation function $R_f(\tau)$,

$$S_f(\nu) = \int_{\mathbb{R}} R_f(\tau) \exp(i2\pi\nu\tau) d\tau, \tag{2.32}$$

provided $R_f(\tau)$ is continuous at $\tau = 0$. The PSD describes the distribution of the signal power in the frequency domain. The total power is given by

$$P_f = \int_{\mathbb{R}} S_f(\nu) d\nu = R_f(0). \tag{2.33}$$

Hence, (2.31) yields

$$P_f = \langle f \rangle^2 \left(1 + \frac{S_c}{NA_e}\right). \tag{2.34}$$

Speckle noise represents random fluctuations about the average signal value $\langle f \rangle$. Thus, the speckle noise power is the variance σ_f^2 of the process f. For weakly stationary processes, we have $P_f = \langle f \rangle^2 + \sigma_f^2$, which in view of (2.34) yields

$$\sigma_f^2 = \langle f \rangle^2 \frac{S_c}{NA_e}. \tag{2.35}$$

Relation (2.35) shows that the noise power is multiplicative in the sense that it is proportional to the average signal power $\langle f \rangle^2$. Consequently, speckle noise cannot be made relatively smaller by increasing the signal power. We also note that the noise power is proportional to S_c. Therefore, the noise can be reduced by reducing the average speckle size. This is intuitively clear since smaller speckle induces smaller fluctuations in the detector signal.

Let us now derive an explicit expression for the power spectral density (2.32). Substituting (2.31) into (2.32), we have

$$S_f(\nu) = \langle f \rangle^2 \left[\delta(\nu) + \frac{S_c}{NA_e} \frac{1}{\|I\|^2} \int_{\mathbb{R}^3} I(\xi, \eta) I(\xi - V\tau, \eta) \exp(i2\pi\nu\tau) d\xi\, d\eta\, d\tau\right], \tag{2.36}$$

where $\delta(\nu)$ is the Dirac delta function. Very often laser beams are symmetric in the scanning direction, that is, $I(-\xi, \eta) = I(\xi, \eta)$. In this case, the PSD can be simplified as

$$S_f(\nu) = \langle f \rangle^2 \left[\delta(\nu) + \frac{S_c}{VNA_e} \frac{1}{\|I\|^2} \int_{\mathbb{R}} \left(\int_{\mathbb{R}} I(\xi, \eta) \exp\left(i\frac{2\pi\nu}{V}\xi\right) d\xi\right)^2 d\eta\right]. \tag{2.37}$$

Expressed in this form, the PSD can be easily computed using FFT and a numerical integration algorithm, which is important from the standpoint of applications.

2.3. Statistical Properties of Differentiated Speckle Noise

In the conventional approach to edge detection using Canny's algorithm, the signal $f(t)$ is differentiated in order to enhance edges. Since differentiation amplifies high frequencies, it is important to understand the statistical properties of differentiated speckle noise. Let f' denote the random process $\{f'(t) \mid t \in \mathbb{R}\}$ where $f'(t)$ is the derivative of $f(t)$. Since f' is also weakly stationary, the power spectral densities of f and f' are related by [34]

$$S_{f'}(\nu) = 4\pi^2\nu^2 S_f(\nu). \tag{2.38}$$

Using (2.36), we find

$$S_{f'}(\nu) = 4\pi^2 \langle f \rangle^2 \frac{S_c}{NA_e} \frac{1}{\|I\|^2} \int_{\mathbb{R}^3} I(\xi,\eta) I(\xi - V\tau, \eta) \nu^2 \exp(i2\pi\nu\tau) d\xi\, d\eta\, d\tau. \tag{2.39}$$

The total power of the process f' is now given by

$$P_{f'} = \int_{\mathbb{R}} S_{f'}(\nu) d\nu = 4\pi^2 \langle f \rangle^2 \frac{S_c}{NA_e} \frac{1}{\|I\|^2} \int_{\mathbb{R}^4} I(\xi,\eta) I(\xi - V\tau, \eta) \nu^2 \exp(i2\pi\nu\tau) d\xi\, d\eta\, d\tau\, d\nu. \tag{2.40}$$

The above expression can be simplified to a double integral provided the intensity distribution satisfies

$$\lim_{|\xi|,|\eta| \to \infty} I(\xi,\eta) = 0, \qquad \sup_{(\xi,\eta)\in\mathbb{R}^2} \left| \frac{\partial I}{\partial \xi} \right| < \infty. \tag{2.41}$$

These conditions are met in all applications since $I(\xi,\eta)$ has bounded partial derivatives, and it rapidly tends to zero away from the beam centre (this is easily verified for Gaussian beams). Assuming conditions (2.41), let us define the function $H_{\xi,\eta}(\tau) = I(\xi - V\tau, \eta)$. Then

$$\int_{\mathbb{R}^2} I(\xi - V\tau, \eta) \nu^2 e^{i2\pi\nu\tau} d\tau\, d\nu = \int_{\mathbb{R}} \nu^2 \widehat{H}_{\xi\eta}(\nu) d\nu, \tag{2.42}$$

where $\widehat{H}_{\xi\eta}(\nu) = \int_{\mathbb{R}} H_{\xi,\eta}(\tau) \exp(i2\pi\nu\tau) d\tau$ is the Fourier transform of $H_{\xi,\eta}(\tau)$. Substituting the identity

$$\frac{d^2 H_{\xi,\eta}}{d\tau^2} = -4\pi^2 \int_{\mathbb{R}} \nu^2 \widehat{H}_{\xi\eta}(\nu) \exp(-i2\pi\nu\tau) d\nu, \tag{2.43}$$

into (2.42), we find

$$\int_{\mathbb{R}^2} I(\xi - V\tau, \eta) \nu^2 \exp(i2\pi\nu\tau) d\tau\, d\nu = -\frac{1}{4\pi^2} \frac{d^2 H_{\xi,\eta}}{d\tau^2}\bigg|_{\tau=0} = -\frac{V^2}{4\pi^2} \frac{\partial^2 I}{\partial \xi^2}. \tag{2.44}$$

Then the integral in (2.40) becomes

$$\int_{\mathbb{R}^4} I(\xi,\eta) I(\xi - V\tau, \eta) \nu^2 \exp(i2\pi\nu\tau) d\xi\, d\eta\, d\tau\, d\nu = -\frac{V^2}{4\pi^2} \int_{\mathbb{R}^2} I(\xi,\eta) \frac{\partial^2 I}{\partial \xi^2} d\xi\, d\eta. \tag{2.45}$$

Using conditions (2.41), a partial integration yields

$$\int_{\mathbb{R}} I(\xi,\eta) \frac{\partial^2 I}{\partial \xi^2} d\xi = -\int_{\mathbb{R}} \left(\frac{\partial I}{\partial \xi} \right)^2 d\xi. \tag{2.46}$$

Finally, combining (2.40), (2.45), and (2.46), we obtain

$$P_{f'} = \langle f \rangle^2 V^2 \frac{S_c}{NA_e} \frac{1}{\|I\|^2} \left\| \frac{\partial I}{\partial \xi} \right\|^2. \tag{2.47}$$

We refer to (2.47) as the total power of differentiated speckle noise. Since $\mathbf{E}[f'(t)] = 0$, the power $P_{f'}$ equals the variance $\sigma_{f'}^2$ of the process f'.

2.4. Example: Elliptical Gaussian Illumination

Many lasers emit beam whose optical field can be approximated by the elliptical Gaussian function

$$U(\xi, \eta) = \sqrt{\frac{2P}{\pi \omega_x \omega_y}} \exp\left[-\left(\frac{\xi^2}{\omega_x^2} + \frac{\eta^2}{\omega_y^2} \right) \right], \tag{2.48}$$

where ω_x and ω_y are the beam radii in the ξ and η directions, and $P = \int_{\mathbb{R}^2} |U(\xi, \eta)|^2 d\xi\, d\eta$ is the beam power. Diffraction causes light waves to spread transversely to the direction of propagation. For a Gaussian beam propagating in free space, the beam size is minimum at some point along the axis, called the beam waist. If ω_{0x} and ω_{0y} are the beam radii at the waist, then at some distance z' measured from the waist, the beam size is given by [36]

$$\omega_x = \omega_{0x} \sqrt{1 + \left(\frac{\lambda z'}{\pi \omega_{0x}^2} \right)^2}, \qquad \omega_y = \omega_{0y} \sqrt{1 + \left(\frac{\lambda z'}{\pi \omega_{0y}^2} \right)^2}. \tag{2.49}$$

Let us calculate the average size of speckle generated by a Gaussian beam. Substituting the beam intensity $I(\xi, \eta) = |U(\xi, \eta)|^2$ from (2.48) into (2.14), we find that the speckle correlation cells have elliptical shape of average area

$$S_c = \pi \left(\frac{\lambda z}{\pi \omega_x} \right) \left(\frac{\lambda z}{\pi \omega_y} \right). \tag{2.50}$$

It is interesting to note that using geometrical considerations, Ennos [37] estimated the average speckle diameter to be $d = 1.2\lambda z / D$ where D is the diameter of the laser beam. For a circular Gaussian beam with $\omega_x = \omega_y = \omega$, the speckle correlation area S_c corresponds to a circle with diameter

$$d_c = 2\sqrt{\frac{S_c}{\pi}} = \frac{2\lambda z}{\pi \omega} \approx 1.27 \frac{\lambda z}{2\omega}. \tag{2.51}$$

This is indeed very close to the estimated value derived in [37] with $D = 2\omega$.

The complex coherence function (2.20) of the moving field is given by

$$\left|\mu_d(x,y,\tau)\right|^2 = \exp\left[-\left(\frac{V\tau}{\omega_x}\right)^2\right]\exp\left[-\left(\frac{\pi}{\lambda z}\right)^2\left((\omega_x x)^2+(\omega_y y)^2\right)\right]. \tag{2.52}$$

The maximum value of $|\mu_d(x,y,\tau)|^2$ is attained at $x = y = 0$. For a fixed value of $\tau > 0$, the "support" of $|\mu_d(x,y,\tau)|^2$ can be defined as the subset $\Omega \subset \mathbb{R}^2$ such that

$$\sup_{(x,y)\in\Omega}\left|\mu_d(x,y,\tau)\right|^2 \le \frac{1}{e^2}\left|\mu_d(0,0,\tau)\right|^2. \tag{2.53}$$

It is easily seen that Ω is the elliptical region defined by

$$\left(\frac{x}{a}\right)^2+\left(\frac{y}{b}\right)^2 \le 1, \tag{2.54}$$

where $a = \sqrt{2}\lambda z/(\pi\omega_x)$ and $b = \sqrt{2}\lambda z/(\pi\omega_y)$. Thus, Ω has the area

$$|\Omega| = 2\pi\left(\frac{\lambda z}{\pi\omega_x}\right)\left(\frac{\lambda z}{\pi\omega_y}\right) = 2S_c, \tag{2.55}$$

where $S_c = (\lambda z)^2/(\pi\omega_x\omega_y)$ is the average speckle size. Since a typical detector aperture contains a large number of speckle cells, the support of μ_d is much smaller than the aperture. This justifies the approximation made in (2.25).

The autocorrelation function (2.30) is given by

$$R_f(\tau) = \langle f\rangle^2\left(1+\frac{S_c}{NA_e}\exp\left[-\left(\frac{V\tau}{\omega_x}\right)^2\right]\right). \tag{2.56}$$

Now, the PSD of the processes f and f' are found to be

$$S_f(\nu) = \int_{\mathbb{R}} R_f(\tau)\exp(i2\pi\nu\tau)d\tau = \langle f\rangle^2\left(\delta(\nu)+\sqrt{\pi}\frac{S_c}{NA_e}\frac{\omega_x}{V}\exp\left[-\left(\frac{\pi\omega_x}{V}\right)^2\nu^2\right]\right), \tag{2.57}$$

$$S_{f'}(\nu) = 4\pi\nu^2 S_f(\nu) = 4\pi^{5/2}\langle f\rangle^2\frac{S_c}{NA_e}\frac{\omega_x}{V}\nu^2\exp\left[-\left(\frac{\pi\omega_x}{V}\right)^2\nu^2\right]. \tag{2.58}$$

Integrating (2.58) over the real line, we obtain the power of differentiated speckle noise

$$P_{f'} = 2\langle f\rangle^2\left(\frac{V}{\omega_x}\right)^2\frac{S_c}{NA_e}, \tag{2.59}$$

where S_c is given by (2.50).

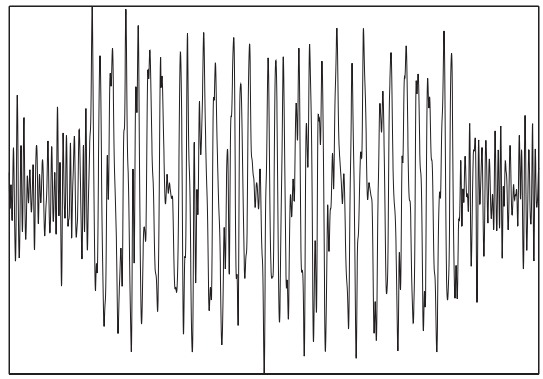

Figure 5: Derivative of a signal corrupted by speckle noise obtained by scanning the bar code in Figure 1.

3. Signal-to-Noise Ratio

Thus far, we considered only signals corrupted by speckle noise when a laser beam scans a surface of uniform reflectance. Next, we turn our attention to signals that result from scanning different configurations of edges. As a toy model, we consider a single edge and an infinite sequence of edges. An edge is defined as a boundary between two regions of different reflectance. The higher reflectance is normalized to one, and the lower reflectance is denoted by $\rho \in [0,1)$. The gray level of a sequence of bars and spaces is modeled by a piecewise constant function $B(\xi)$. The photodetector signal is now given by

$$f(t) = s(t) + n(t), \tag{3.1}$$

where $s(t)$ is the noise-free signal, and $n(t)$ is speckle noise. The noise-free signal is the convolution

$$s(t) = f_0 \int_{\mathbb{R}} B(Vt - \xi) L(\xi) d\xi, \tag{3.2}$$

where

$$L(\xi) = \frac{1}{P} \int_{\mathbb{R}} I(\xi, \eta) d\eta \tag{3.3}$$

is the line spread function of the beam, and $P = \int_{\mathbb{R}^2} I(\xi,\eta) d\xi\, d\eta$ is the beam power. Note that if the reflectance is constant, $B(\xi) = \rho$, then $\langle f \rangle = s(t) = f_0\rho$; hence, f_0 is the maximum value of $\langle f \rangle$ corresponding to $\rho = 1$. In view of (2.17), we have $f_0 = P\mathcal{R}\Omega_d$.

Information about edges is extracted from the derivative of $f(t)$. Figure 5 shows the derivative of a signal corrupted by speckle noise obtained by scanning the bar code in Figure 1. Suppose for the moment that the signal is noise-free, that is, $f(t) = s(t)$. Then

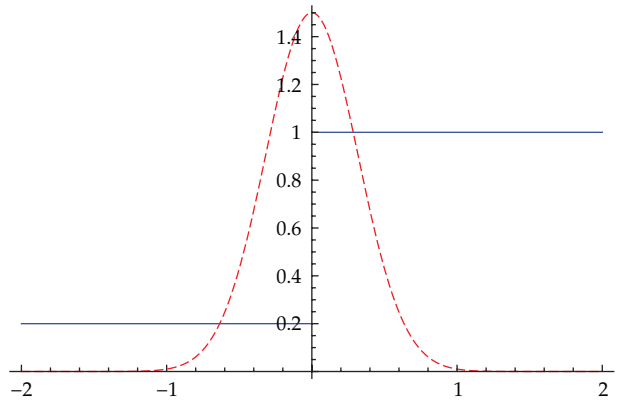

Figure 6: Derivative of a photodetector signal (−−) generated by a Gaussian beam scanning a single edge at $\xi = 0$.

the local extrema of $s'(t)$ above a certain threshold correspond to edges, as illustrated in Figures 6 and 7. Thus, it is appropriate to define the signal S by

$$S = \max_t \left| s'(t) \right|. \tag{3.4}$$

Accordingly, we define the signal-to-noise ratio (SNR) to be

$$\text{SNR} = \left(\frac{S}{\sigma_{n'}} \right)^2, \tag{3.5}$$

where $\sigma_{n'}^2$ denotes the power of differentiated speckle noise. We are interested in obtaining a lower bound for SNR when the speckle noise power is maximal. This happens when the beam is scattered from the region of higher reflectance $\rho = 1$ in which case $\langle f \rangle = f_0$. Combining (2.14) and (2.47), we can express $\sigma_{n'}^2$ as

$$\sigma_{n'}^2 = f_0^2 V^2 \frac{(\lambda z)^2}{NA_e} \frac{1}{P^2} \left\| \frac{\partial I}{\partial \xi} \right\|^2. \tag{3.6}$$

Let us now consider specific examples.

3.1. One Edge

The gray level of a single edge is given by

$$B(\xi) = \rho + (1 - \rho) H(\xi), \tag{3.7}$$

where $H(\xi)$ is the Heaviside step function: $H(\xi) = 0$ if $\xi < 0$ and $H(\xi) = 1$ if $\xi \geq 0$. Then $B'(\xi) = (1 - \rho)\delta(\xi)$; hence, (3.2) leads to

$$s'(t) = (1 - \rho) f_0 V L(Vt). \tag{3.8}$$

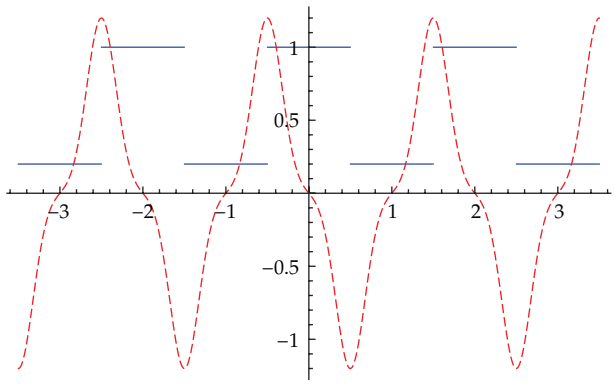

Figure 7: Derivative of a photodetector signal (−−) generated by a Gaussian beam scanning an infinite sequence of edges.

The line spread function has a global maximum at its centre, and thus, the signal S yields

$$S = \max_t \left| s'(t) \right| = (1-\rho) f_0 V L(0). \tag{3.9}$$

Therefore, a lower bound for SNR is given by

$$\mathrm{SNR}_1 = \left(\frac{S}{\sigma_{n'}} \right)^2 = (1-\rho)^2 P^2 \, \frac{NA_e}{(\lambda z)^2} \frac{L^2(0)}{\|\partial I / \partial \xi\|^2}. \tag{3.10}$$

3.2. *Infinite Sequence of Edges*

Consider an infinite sequence of black and white bars of width D where the middle of a white bar is placed at $\xi = 0$, as shown in Figure 7. The gray level is represented by

$$B(\xi) = \rho + (1-\rho) \sum_{k=-\infty}^{\infty} (-1)^{k+1} H\left(\xi - (2k+1)\frac{D}{2} \right). \tag{3.11}$$

The distributional derivative of $B(\xi)$ is the generalized function

$$B'(\xi) = (1-\rho) \sum_{k=-\infty}^{\infty} (-1)^{k+1} \delta\left(\xi - (2k+1)\frac{D}{2} \right), \tag{3.12}$$

which together with (3.2) yields

$$s'(t) = (1-\rho) f_0 V \sum_{k=-\infty}^{\infty} (-1)^{k+1} L\left(Vt - (2k+1)\frac{D}{2} \right). \tag{3.13}$$

We show that under certain mild assumptions which are satisfied in applications, the maximum of $|s'(t)|$ is attained at the point $Vt = D/2$. Let us expand $B'(\xi)$ into generalized Fourier series

$$B'(\xi) = i\frac{1-\rho}{D}\sum_{k=-\infty}^{\infty}(-1)^k \exp\left(i2\pi\frac{2k+1}{2D}\xi\right), \tag{3.14}$$

where $i = \sqrt{-1}$. Using relation (3.14), we find that the signal derivative is given by

$$s'(t) = i(1-\rho)\frac{f_0 V}{D}\sum_{k=-\infty}^{\infty}(-1)^k \exp\left(i2\pi\frac{2k+1}{2D}Vt\right)\widehat{L}\left(-\frac{2k+1}{2D}\right), \tag{3.15}$$

where

$$\widehat{L}(\nu) = \int_{\mathbb{R}} L(\xi)\exp(i2\pi\nu\xi)d\xi \tag{3.16}$$

is the Fourier transform of $L(\xi)$. If the laser beam is symmetric in the scanning direction, then $L(\xi)$ is an even function which implies $\widehat{L}(-\nu) = \widehat{L}(\nu)$. One can use the symmetry of $\widehat{L}(\nu)$ to obtain

$$s'(t) = 2(1-\rho)\frac{f_0 V}{D}\sum_{k=0}^{\infty}(-1)^{k+1}\sin\left(\pi(2k+1)\frac{Vt}{D}\right)\widehat{L}\left(\frac{2k+1}{2D}\right). \tag{3.17}$$

Most often laser beams used in scanning applications have a nearly Gaussian profile. Thus, the Fourier transform of the line spread function may be assumed to be nonnegative, $\widehat{L}(\nu) \geq 0$ for all $\nu \in \mathbb{R}$. Since $\sin((\pi/2)(2k+1)) = (-1)^k$, it follows from (3.17) that the maximum value of $|s'(t)|$ is attained at $Vt = D/2$, which yields

$$S = \max_t |s'(t)| = 2(1-\rho)\frac{f_0 V}{D}\sum_{k=0}^{\infty}\widehat{L}\left(\frac{2k+1}{2D}\right). \tag{3.18}$$

Finally, using (3.6) and (3.18), we find a lower bound for SNR to be

$$\mathrm{SNR}_\infty = \left(\frac{S}{\sigma_n'}\right)^2 = 4(1-\rho)^2 P^2 \frac{NA_e}{(\lambda z)^2}\frac{1}{D^2}\frac{\left[\sum_{k=0}^{\infty}\widehat{L}((2k+1)/2D)\right]^2}{\|\partial I/\partial\xi\|^2}. \tag{3.19}$$

3.3. SNR for Gaussian Optical Field

In the following, we illustrate the estimates of SNR for a beam with Gaussian intensity. We also describe qualitative dependence of SNR on the scan distance z. The line spread function of the Gaussian field (2.48) is given by

$$L(\xi) = \sqrt{\frac{2}{\pi}}\frac{1}{\omega_x}\exp\left[-2\left(\frac{\xi}{\omega_x}\right)^2\right], \tag{3.20}$$

and the L^2-norm of $\partial I/\partial\xi$ is

$$\left\|\frac{\partial I}{\partial \xi}\right\|^2 = \frac{2}{\pi}\frac{P^2}{\omega_x^3\omega_y}. \tag{3.21}$$

Substituting (3.20) and (3.21) into (3.10), we find

$$\mathrm{SNR}_1 = (1-\rho)^2\frac{NA_e}{(\lambda z)^2}\omega_x\omega_y. \tag{3.22}$$

In order to find SNR_∞, we need the Fourier transform of the line spread function $L(\xi)$,

$$\widehat{L}(\nu) = \exp\left(-\frac{1}{2}(\pi\omega_x)^2\nu^2\right). \tag{3.23}$$

Then, (3.19) yields

$$\mathrm{SNR}_\infty = 2\pi(1-\rho)^2\omega_x\omega_y\left(\frac{\omega_x}{D}\right)^2\frac{NA_e}{(\lambda z)^2}\left[\sum_{k=0}^{\infty}\exp\left(-\frac{\pi^2}{8}\left(\frac{\omega_x}{D}\right)^2(2k+1)^2\right)\right]^2. \tag{3.24}$$

We note that SNR_∞ depends on the spot-to-bar ratio $r = 2\omega_x/D$ which plays an important role in bar code signal analysis. In most cases, $1 \le r \le 3$; hence, the series in (3.24) converges very quickly, and it suffices to keep only the first few terms. This is intuitively clear since the edges far away from the beam do not contribute to the SNR. Figure 8 shows dependence of SNR_∞ on the spot-to-bar ratio $r \in [1,3]$. It is apparent that SNR_∞ is maximum when $r = 1$ which implies that narrow beams ($r = D$) have better SNR than wide beams ($r = 3D$).

3.4. Dependence of SNR on Scan Distance

Recall that the beam size changes along the propagation axis according to (2.49). Thus, the SNR is a function of the scan distance z, which we investigate next. Suppose the beam waist is at a distance z_w from the photodetector. Since the laser is placed next to the photodetector, the scan distance can be written as $z = z_w + z'$ where z' is the distance from the waist to

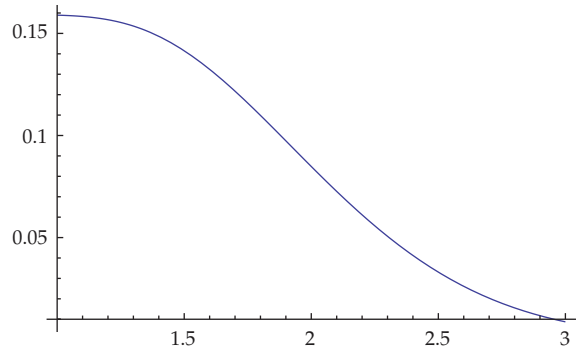

Figure 8: Function $f(r) = (r/2)^2\left[\sum_{k=0}^{2} \exp(-(\pi^2/8)(2k+1)^2(r/2)^2)\right]^2$.

the scattering plane. For simplicity, we assume that the beam is circular, that is, $\omega_{0x} = \omega_{0y} = \omega_0$. Then in view of (2.49),

$$\omega_x = \omega_y = \omega_0\sqrt{1 + \left(\frac{\lambda z'}{\pi\omega_0^2}\right)^2}. \tag{3.25}$$

Let us define the dimensionless variables $u = \lambda z'/\omega_0^2$ and $u_w = \lambda z_w/\omega_0^2$. Substituting (3.25) into (3.22) and rearranging terms, we obtain

$$\mathrm{SNR}_1 = (1-\rho)^2 \frac{NA_e}{\omega_0^2} f(u), \tag{3.26}$$

where

$$f(u) = \frac{1 + (u/\pi)^2}{(u+u_w)^2}, \quad -u_w < u < \infty. \tag{3.27}$$

For a particular scanner, the waist location z_w is fixed (it is close to the output surface of the laser). Thus, (3.26) provides dependence of SNR_1 on the scan distance $z = z_w + z'$. The function $f(u)$ is decreasing for $-u_w < u < \pi^2/u_w$ and increasing for $u > \pi^2/u_w$. It has a local minimum at $u_{\min} = \pi^2/u_w$, that is, at $z'_{\min} = \pi^2\omega_0^4/(\lambda^2 z_w)$. The lowest value of SNR_1 is attained at $z_{\min} = z'_{\min} + z_w$ and

$$(\mathrm{SNR}_1)_{\min} = (1-\rho)^2 \frac{NA_e}{\omega_0^2} \frac{1}{\pi^2 + (\lambda z_w/\omega_0^2)^2}. \tag{3.28}$$

Typical values of the wavelength and spot size are $\lambda = 670 \cdot 10^{-9}$ m, $\omega_0 \approx 10^{-3}$ m, and $z_w \approx 10^{-1}$ m. For these values of λ, ω_0, and z_w, we have $z_{\min} \gg z_w$; hence, the minimum occurs far beyond the working range of a scanner. Consequently, for application purposes, we may consider SNR_1 simply a decreasing function of z, which implies that better SNR is achieved at shorter scan distances.

The same qualitative behaviour can also be deduced by analyzing SNR_∞. Let us define $Q = \exp[-(\pi^2/8)(r/2)^2]$ where $r = 2\omega_x/D$ is the spot-to-bar ratio at distance z. Then (3.24) can be written as

$$\mathrm{SNR}_\infty = 2\pi(1-\rho)^2\omega_x\omega_y\left(\frac{\omega_x}{D}\right)^2\frac{NA_e}{(\lambda z)^2}\left[\sum_{k=0}^{\infty}Q^{(2k+1)^2}\right]^2. \tag{3.29}$$

We wish to find an approximate expression for SNR_∞. Define $Q_0 = \exp[-(\pi^2/8)(r_0/2)^2]$ where $r_0 = 2\omega_0/D$ is the spot-to-bar ratio at the waist. It is easily seen that for $r_0 \in [1,3]$, we can make the approximation

$$\left[\sum_{k=0}^{\infty}Q_0^{(2k+1)^2}\right]^2 = Q_0^2 + 2Q_0^{10} + \text{higher-order terms} \approx Q_0^2. \tag{3.30}$$

Since $\omega_0 \le \omega_x$, we have $0 < Q \le Q_0 < 1$; hence, the approximation (3.30) also holds for Q. Therefore, SNR_∞ can be approximated by

$$\mathrm{SNR}_\infty = 2\pi(1-\rho)^2\omega_x\omega_y\left(\frac{\omega_x}{D}\right)^2\frac{NA_e}{(\lambda z)^2}Q^2, \tag{3.31}$$

for all $r_0 \in [1,3]$. Now, substituting (3.25) into (3.31), we find

$$\mathrm{SNR}_\infty = 2\pi(1-\rho)^2\frac{NA_e}{D^2}g(u), \tag{3.32}$$

where

$$g(u) = \frac{1}{(u+u_w)^2}\left[1+\left(\frac{u}{\pi}\right)^2\right]^2\exp\left[-\frac{\pi^2}{4}\left(\frac{r_0}{2}\right)^2\left(1+\left(\frac{u}{\pi}\right)^2\right)\right]. \tag{3.33}$$

The behaviour of $g(u)$ is more complex than $f(u)$, and it depends on the exact values of the parameters $u_w = \lambda z_w/\omega_0^2$ and $r_0 = 2\omega_0/D$. For typical values of λ, ω_0, and z_w as given above, the function $g(u)$ is monotonically decreasing for all $r_0 \in [1,3]$. This means that SNR is larger at shorter scan distances. Since a laser beam spreads as it propagates, this is in agreement with earlier finding that a better SNR is achieved for smaller spot-to-bar ratios $r = 2\omega_x/D$.

4. Edge Localization Error

In this section, we investigate the edge localization error in bar code signals caused by speckle noise. Suppose the edges are located at $X_1 < X_2 < \cdots < X_n$, so the gray level of a bar code is represented by

$$B(\xi) = \rho + (1-\rho)\sum_{k=1}^{n}(-1)^{k+1}H(\xi - X_k). \tag{4.1}$$

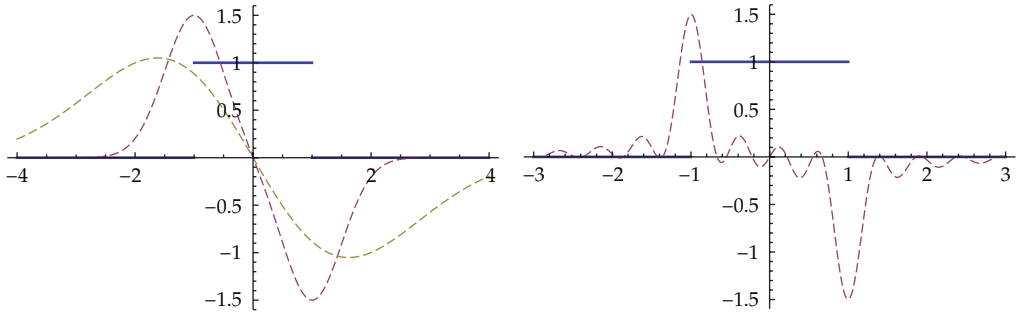

Figure 9: Noise-free signal $s'(t)$ (−−) generated by different scanning beams: (a) Gaussian beam with $\omega_x = 1$ and $\omega_x = 3$, (b) beam with intensity distribution given by (4.2).

As explained earlier, the observed signal is given by (3.1), and the edges are detected by finding the local extrema of $f'(t)$. There are several difficulties related to this approach. First, a local extremum of $f'(t)$ may represent a noised edge, which is clearly seen in Figure 5. Second, even in noise-free conditions, an edge may be erroneously detected due to convolution distortion (blur), or due to a specific shape of the line spread function. Figure 9(a) shows a single bar with gray level $B(\xi) = H(\xi + 1) - H(\xi - 1)$ scanned by the Gaussian beam (2.48) at two different scales: $\omega_x = 1$ and $\omega_x = 3$. It is evident that the distance between the local extrema of $s'(t)$ increases with ω_x, which distorts the apparent bar width. In general, the neighbouring edges interact with each other, and the convolution distortion becomes more complicated. For a modification of the standard technique for edge detection which deals with severely blurred bar codes, see [20] and [38]. If the line spread function is not Gaussian, then the local extrema of $s'(t)$ may lead to false edges as in Figure 9(b). This figure shows a single bar scanned by the beam with intensity

$$I(\xi, \eta) = I_0 \exp\left(-2\frac{r^2}{\omega^2}\right) J_0^2\left(\frac{2\pi}{\lambda}\theta r\right), \tag{4.2}$$

where $r = \sqrt{\xi^2 + \eta^2}$, and J_0 is the zero-order Bessel function of the first kind. Due to its slow divergence, this kind of beam is used in some scanners for long-range applications. These two effects combined together make edge detection even more difficult.

In our analysis, we assume that the convolution distortion is sufficiently small, and we focus our attention on edge localization error caused by speckle noise only. Suppose that the signal $f(t) = s(t)+n(t)$ is given by (3.1)–(3.3). In the preprocessing stage, the derivative $f'(t)$ is filtered by a linear filter with impulse response $h(t)$. An algorithm for selecting optimal filter scale based on the narrow element estimate is presented in [2]. Applications of multiscale algorithms in edge detection can be found in [13–15, 39]. After filtering, the observed signal becomes

$$g(t) = \int_{\mathbb{R}} h(t-\tau)s'(\tau)d\tau + \int_{\mathbb{R}} h(t-\tau)n'(\tau)d\tau. \tag{4.3}$$

We denote $g_0(t) = (h * s')(t)$ and $g_n(t) = (h * n')(t)$ where $*$ is the convolution operator $(x * y)(t) = \int_{\mathbb{R}} x(t-\tau)y(\tau)d\tau$. Since the derivative of speckle noise is a weakly stationary process, so is the process $g_n = \{g_n(t) \mid t \in \mathbb{R}\}$. Now, we pose the following problem: given spectral characteristics of the process $n = \{n(t) \mid t \in \mathbb{R}\}$ estimate the error in locating the edges in (4.1). In general, this is a fairly complicated problem, so we introduce several simplifying assumptions. Let us examine more closely the noise-free signal $g_0(t) = (h * s')(t)$. By substituting (4.1) into (3.2), we obtain

$$g_0(t) = f_0(1-\rho)V \sum_{k=1}^{n} (-1)^{k+1}(h * L_V)(t - T_k), \tag{4.4}$$

where $L_V(t) = L(Vt)$ and $T_k = X_k/V$ are the edge positions in time domain. The edge locations in noise-free conditions are approximated by solutions of the nonlinear equation $g_0'(t) = 0$, that is,

$$\sum_{k=1}^{n} (-1)^{k+1}(h * L_V)'(t - T_k) = 0. \tag{4.5}$$

The number of solutions t_k of (4.5) is usually greater than the number of edges, depending on the exact shape of the line spread function. Furthermore, $t_k \neq T_k$ due to convolution distortion. In our analysis, we will assume that the data $\{t_k\}_{k=1}^n$ is given and is sufficient to perform decoding, that is, $t_{k+1} - t_k \approx T_{k+1} - T_k$ for all k. This is true if the support of $L(\xi)$ is comparable in size with $\min_k |X_{k+1} - X_k|$, the smallest bar or space.

If the signal is corrupted by noise, we are interested in solutions of the equation

$$g_0'(t) + g_n'(t) = 0, \tag{4.6}$$

which represent small random perturbations of the noise-free solutions $\{t_k\}_{k=1}^n$. Let t be a solution of (4.6), and let $e_k = t - t_k$ be a random error associated to t_k. The statistical properties of the random variable e_k depend on the process $n = \{n(t) \mid t \in \mathbb{R}\}$. It is shown in [40] that for small errors the expected value of e_k is $\mathbf{E}[e_k] = 0$. Furthermore, the second moment of e_k is given by

$$\mathbf{E}\left[e_k^2\right] = \left(\frac{4\pi^2}{f_0(1-\rho)V}\right)^2 \frac{\int_{\mathbb{R}} \nu^4 \left|\widehat{h}(\nu)\right|^2 S_n(\nu)d\nu}{\left[\sum_{i=1}^{n} (-1)^{i+1}(h * L_V)''(t_k - T_i)\right]^2}, \tag{4.7}$$

where $\widehat{h}(\nu)$ is the Fourier transform of $h(t)$, and $S_n(\nu)$ is the power spectral density of n. We define the edge position error to be the standard deviation

$$\delta_k = V\sqrt{\mathbf{E}\left[e_k^2\right] - \mathbf{E}^2[e_k]} = \frac{4\pi^2}{f_0(1-\rho)} \frac{\left[\int_{\mathbb{R}} \nu^4 \left|\widehat{h}(\nu)\right|^2 S_n(\nu)d\nu\right]^{1/2}}{\left|\sum_{i=1}^{n} (-1)^{i+1}(h * L_V)''(t_k - T_i)\right|}. \tag{4.8}$$

The above relation shows that δ_k depends on the spectral characteristics of the noise n as well as the positions of edges in a bar code symbol. The function $(h * L_V)''(t)$ often decays rapidly to zero as $|t|$ grows, that is, $(h * L_V)''(t_k - T_i) \approx 0$ when $|t_k - T_i|$ is large. Hence, only the nearest neighbours of edge k contribute to the error δ_k.

4.1. Speckle Noise and Edge Localization Error for Gaussian Optical Field

As noted earlier, the laser beam profile most often used in scanning is approximately the Gaussian function. Hence, it is instructive to study the edge localization error when the optical field is given by (2.48). We assume that the filer impulse response is given by

$$h(t) = \frac{1}{\sqrt{2\pi}\sigma} \exp\left[-\frac{1}{2}\left(\frac{t}{\sigma}\right)^2\right]. \tag{4.9}$$

This type of filter acts as a low-pass filter and is commonly used in Canny's algorithm for edge detection [19]. It is known that the Gaussian filter does not create false edges as the scale σ increases [41]. The frequency response of the filter is given by $\widehat{h}(\nu) = \exp[-2(\pi\sigma\nu)^2]$. Furthermore, the PSD of speckle noise is given by $S_n(\nu) = S_f(\nu) - \langle f \rangle^2 \delta(\nu)$; hence, in view of (2.57),

$$S_n(\nu) = f_0^2 \sqrt{\pi} \frac{S_c}{NA_e} \frac{\omega_x}{V} \exp\left[-\left(\frac{\pi\omega_x}{V}\right)^2 \nu^2\right]. \tag{4.10}$$

A straightforward computation yields

$$\int_{\mathbb{R}} \nu^2 \left|\widehat{h}(\nu)\right|^2 S_n(\nu) d\nu = \frac{3}{4\pi^4} f_0^2 \frac{S_c}{NA_e} \left(\frac{V}{\omega_x}\right)^4 \frac{1}{\beta^5}, \tag{4.11}$$

where $\beta = \sqrt{1 + 4(V\sigma/\omega_x)^2}$. By convolving the impulse response $h(t)$ with the line spread function (3.20), we obtain

$$(h * L_V)(t) = \sqrt{\frac{2}{\pi}} \frac{1}{\beta\omega_x} \exp\left[-2\left(\frac{Vt}{\beta\omega_x}\right)^2\right]. \tag{4.12}$$

This leads immediately to

$$(h * L_V)''(t) = \sqrt{\frac{8}{\pi}} \frac{V^2}{(\beta\omega_x)^3} H_2\left(\sqrt{2}\frac{Vt}{\beta\omega_x}\right) \exp\left[-2\left(\frac{Vt}{\beta\omega_x}\right)^2\right], \tag{4.13}$$

where $H_2(x) = 4x^2 - 2$ is the Hermite polynomial of degree two. Substituting (4.11) and (4.13) into (4.8), we find

$$\delta_k = \frac{1}{1-\rho}\sqrt{\frac{3\pi S_c}{2NA_e}}\,\frac{\sqrt{\beta}\omega_x}{\left|\sum_{i=1}^{n}(-1)^{i+1}H_2\left(\sqrt{2}(x_k - X_i/\beta\omega_x)\right)\exp\left[-2(x_k - X_i/\beta\omega_x)^2\right]\right|}, \quad (4.14)$$

where $x_k = Vt_k$ and $X_k = VT_k$. Recall that $\{X_k\}_{k=1}^n$ are true edge positions and that $\{x_k\}_{k=1}^n$ are solutions of (4.5) which in our case yields

$$\sum_{k=1}^{n}(-1)^{k+1}(t - T_k)\exp\left[-2\left(\frac{V}{\beta\omega_x}\right)^2(t - T_k)^2\right] = 0. \quad (4.15)$$

This equation has exactly n distinct solutions $t_1 < t_2 < \cdots < t_n$. Convolution distortion is negligible if $\beta\omega_x \leq \min_k|X_{k+1} - X_k|$, the smallest bar or space. In this case, $t_k \approx T_k$ to a very good approximation; otherwise, (4.15) must be solved numerically.

The factor β is responsible for deviations of δ_k from the value it would have in the absence of a filter. Indeed, $\lim_{\sigma\to 0^+}\delta_k = \delta_k^{(0)}$ where

$$\delta_k^{(0)} = \frac{1}{1-\rho}\sqrt{\frac{3\pi S_c}{2NA_e}}\,\frac{\omega_x}{\left|\sum_{i=1}^{n}(-1)^{i+1}H_2\left(\sqrt{2}(x_k - X_i)/\omega_x\right)\exp\left[-2((x_k - X_i)/\omega_x)^2\right]\right|} \quad (4.16)$$

is the error obtained from (4.8) if $h(t)$ is replaced by the Dirac function $\delta(t)$.

4.2. Susceptibility of Bar Code Symbols to Edge Localization Errors

Relation (4.16) is very useful in studying the distribution of edge localization errors caused by speckle noise in different bar code symbols. When convolution distortion is small, that is, $x_k \approx X_k$ for all k, the edge localization errors in a given bar code symbol can be analyzed as follows.

The width of a bar or space in a symbol is a multiple of a unit width D, called module. We may assume that the edges are located at

$$X_1 = 0,\ X_2 = p_1D,\ X_3 = (p_1 + p_2)D, \ldots,\ X_n = \left(\sum_{k=1}^{n-1}p_k\right)D. \quad (4.17)$$

A message stored in a bar code is encoded in the digital bar pattern $\mathcal{S} = (p_1, p_2, \ldots, p_{n-1})$. As explained earlier, the possible values of p_k in the UPCA symbology are $p_k = 1, 2, 3, 4$. Each integer between 0 and 9 is encoded as a sequence (p_1, p_2, p_3, p_4) where $\sum_{k=1}^{4}p_k = 7$. Table 1 shows encodation patterns for integers $0, 1, \ldots, 9$. For more details on different symbologies, see [1]. For convenience, we define $d_k = \sum_{i=1}^{k-1}p_i$, $2 \leq k \leq n$, and set $d_1 = 0$. Then the distance between a pair of edges is $X_k - X_i = (d_k - d_i)D$. We introduce the spot-to-bar ratio $r = 2\omega_x/D$

as a measure of the beam size $2\omega_x$ relative to the smallest bar or space. Using (4.16), the edge localization error relative to the module size can be written as

$$\frac{\delta_k^{(0)}}{D} = \frac{1}{1-\rho}\sqrt{\frac{3\pi S_c}{8NA_e}}\,\frac{r}{\left|\sum_{i=1}^{n}(-1)^{i+1}H_2\left(\sqrt{8}(d_k-d_i)/r\right)\exp\left[-8((d_k-d_i)/r)^2\right]\right|}, \tag{4.18}$$

where we have used $x_k = X_k$.

The relative error $\delta_k^{(0)}/D$ can be used to define susceptibility of a bar code symbol to edge localization errors. Here, we should take into account that a large error in the position of a single edge can make the entire bar code unreadable. This suggests that susceptibility should be defined by

$$\|\mathcal{S}\| = \max_k \left|\frac{\delta_k^{(0)}}{D}\right|. \tag{4.19}$$

Note that $\|\mathcal{S}\|$ is proportional to $(1-\rho)^{-1}\sqrt{3\pi S_c/(8NA_e)}$ which depends only on the physical characteristics of the system. Hence, we introduce susceptibility which is intrinsic to the bar code symbol alone by $\|\mathcal{S}\|_0 = \max_k |E_k(\mathcal{S})|$ where

$$E_k(\mathcal{S}) = \frac{r}{\left|\sum_{i=1}^{n}(-1)^{i+1}H_2\left(\sqrt{8}(d_k-d_i)/r\right)\exp\left[-8((d_k-d_i)/r))^2\right]\right|}. \tag{4.20}$$

The measure $\|\mathcal{S}\|_0$ depends only on the relative positions of edges, that is, the message content of the bar code, and the spot-to-bar ratio r. Figure 10 shows the distribution of errors $E_k(\mathcal{S})$ when $\mathcal{S}$ encodes the message "012345678905." Investigation of the error distributions for a large number of UPCA symbols reveals that this is a typical result: the errors $E_k(\mathcal{S})$ cluster around the values 0.5, 0.35, and 0.27. Hence, all UPCA symbols have approximately the same maximum error $\|\mathcal{S}\|_0 = 0.5$ which is about twice as large as the minimum error. One can similarly study the distribution of errors in other popular symbologies, such as code 39 and code 128, and for different beam profiles. We remark that if the approximation $x_k \approx X_k$ is not valid, then the apparent edge positions x_k must be computed numerically from (4.15).

5. Applications to System Design and Open Problems

The theoretical analysis presented here can be used as a guide in system design. Here, we discuss several possibilities that will be investigated in future work. Performance of a bar code scanner greatly depends on how the laser beam is focused. Beam focusing is guided by two key requirements imposed on the scanning device:

(i) bar code density, that is, the smallest bar code a scanner can read,

(ii) working range within which bar codes can be decoded.

The working range is estimated by using the modulation transfer function (MTF) of the scanning beam. Let $L(\xi)$ be the line spread function of the beam, and let ν_0 be the spatial

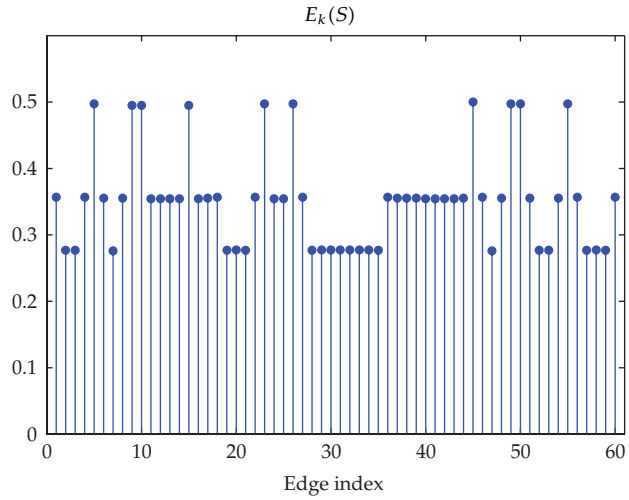

Figure 10: Edge position errors $E_k(\mathcal{S})$ for UPCA symbol encoding the message "012345678905."

frequency of the smallest bar or space we wish to read ($\nu_0 = 1/(2D)$). For symmetric beams, the MTF is given by MTF $= |\widehat{L}(\nu_0)|$. Since the beam intensity changes with scan distance z, so does the MTF. By plotting the MTF as a function of z, one can estimate the region of decoding as the interval in which the MTF is greater than some predefined value. This analysis, however, takes into account only degradation of the image due to finite size of the beam.

We propose an alternative approach which also takes into account the effects of speckle noise on decoding process. Bar code decoding is based on the distance between two adjacent edges. Suppose the edges are located at x_k and x_{k+1}, where $x_k = Vt_k$ are solutions of (4.5). The convolution distortion of a bar (space) between the edges X_k and X_{k+1} is defined by

$$C_k = (x_{k+1} - x_k) - (X_{k+1} - X_k) = \Delta x_k - \Delta X_k. \tag{5.1}$$

A bar code can be decoded if the maximum error of a detected bar (space) width is less than some value σ_B, usually $\sigma_B = B/2$. Then, in noise-free conditions, we demand that

$$\max_k |C_k| \le \sigma_B. \tag{5.2}$$

Now, suppose the signal is corrupted by speckle noise. Then the edge position x_k becomes a random variable $\overline{x}_k = x_k + \overline{e}_k$ where $\overline{e}_k$ is the error in space domain associated with speckle noise (i.e., $\overline{e}_k = Ve_k$). The detected bar (space) width is given by $\Delta\overline{x}_k = \overline{x}_{k+1} - \overline{x}_k = \Delta x_k + \overline{e}_{k+1} - \overline{e}_k$. Since $\mathbf{E}[\overline{e}_k] = 0$, the variance of the detected width is

$$\operatorname{var}(\Delta\overline{x}_k) = \mathbf{E}\left[(\overline{e}_{k+1} - \overline{e}_k)^2\right]. \tag{5.3}$$

Using the Cauchy-Schwartz inequality $\mathbf{E}^2[\overline{e}_{k+1}\overline{e}_k] \le \mathbf{E}[\overline{e}_{k+1}^2]\mathbf{E}[\overline{e}_k^2]$, we obtain $\operatorname{var}(\Delta\overline{x}_k) \le (\delta_{k+1} + \delta_k)^2$ where δ_k is the edge position error defined by (4.8). Therefore, the standard

deviation of $\Delta\overline{x}_k$ is bounded by $\delta_{k+1} + \delta_k$. This suggests that the condition (5.2) should be replaced by

$$\max_k(|C_k| + \delta_{k+1} + \delta_k) \leq \sigma_B. \tag{5.4}$$

The above criteria for bar code decoding also takes into account the effect of filtering since both C_k and δ_k depend on the filter impulse response $h(t)$.

As seen in Section 2, the intensity of a laser beam depends on the scan distance z. The change in the scan distance affects the convolution distortion and the edge position error caused by speckle noise. Therefore, the quantity defined by $J_k(z) = |C_k(z)| + \delta_{k+1}(z) + \delta_k(z)$ is a function of z. It follows that the working range of a scanner can be defined as the interval $[z_1, z_2]$ such that

$$\max_k J_k(z) \leq \sigma_B \quad \forall z \in [z_1, z_2]. \tag{5.5}$$

Another possible use of the above inequality is beam focusing. Since $J_k(z)$ depends on the beam intensity $I(\xi, \eta)$, for a desired interval $[z_1, z_2]$, one should try to design a beam such that (5.5) holds. This condition can also be used to optimize the filter impulse response $h(t)$. These considerations lead to certain variational problems that warrant further investigation.

6. Conclusion

In this paper, we reviewed the effects of speckle noise on bar code decoding. We have shown that when the scattering surface has uniform reflectance, speckle noise is a weakly stationary random process. We derived expressions for the autocorrelation function and power spectral density of the noise in terms of intensity distribution of the scanning beam. We have also derived estimates for a lower bound of signal-to-noise ratio when the signal is obtained by scanning a single edge and an infinite sequence of edges. In the last part of the paper, we investigated the edge localization error caused by speckle noise. We derived a first-order approximation of the error and showed that it depends on the spectral characteristics of the noise as well as relative positions of the edges in a bar code symbol. The results derived here are used to propose alternative criteria for system optimization. We have also pointed to some open problems in systems design that could be studied using the presented analysis. Throughout the paper, the theory was illustrated by analytical examples when a scanning beam has Gaussian intensity.

List of Symbols

$\|\cdot\|$: L^2-norm on $\mathbb{R}^2$
$A(x, y)$: Photodetector response function
A_e: Effective aperture area
$B(\xi)$: Gray level of a bar code
C_k: Convolution distortion
D: Bar code module
δ_k: Standard deviation of edge position error

e_k:	Edge position error
$f(t)$:	Photodetector signal
$I(\xi, \eta)$:	Intensity distribution of incident beam
$I_s(x, y)$:	Intensity distribution of a static speckle pattern
$I_{ds}(x, y, t)$:	Intensity distribution of a dynamic speckle pattern
$\langle I_s \rangle$:	Expected value of $I_s(x, y)$
$L(\xi)$:	Line spread function
λ:	Optical wavelength
$\mu(x, y)$:	Complex coherence function of a static optical field
$\mu_d(x, y, \tau)$:	Complex coherence function of a moving optical field
P:	Beam power
P_f:	Total power of photodetector signal
$\mathcal{R}$:	Optical-to-electrical signal conversion factor
$R_s(x_1, y_1; x_2, y_2)$:	Autocorrelation function of $I_s(x, y)$
$R_{ds}(x_1, y_1; x_2, y_2; t_2, t_1)$:	Autocorrelation function of $I_{ds}(x, y; t)$
$R_f(t_1, t_2)$:	Autocorrelation function of the photodetector signal $f(t)$
$R_A(x, y)$:	Autocorrelation function of the photodetector response $A(x, y)$
$\mathcal{S}$:	Digital bar pattern
$S_f(\nu)$:	Power spectral density of photodetector signal
$S_{f'}(\nu)$:	Power spectral density of differentiated speckle noise
S_c:	Speckle correlation area
σ_f^2:	Speckle noise power
$\sigma_{f'}^2$:	Differentiated speckle noise power
SNR:	Signal-to-noise ratio
$U(\xi, \eta)$:	EM field in the scattering plane
X_k:	Edge positions in space domain.

Acknowledgment

This research was supported by the Croatian Ministry of Science under Grant no. 0023003.

References

[1] R. C. Palmer, *The Bar Code Book*, Helmers Publishing, Peterborough, UK, 4th edition, 2001.
[2] S. Krešić-Jurić, D. Madej, and F. Santosa, "Applications of hidden Markov models in bar code decoding," *Pattern Recognition Letters*, vol. 27, no. 14, pp. 1665–1672, 2006.
[3] L. Rabiner and B. Juang, *Fundamentals of Speech Recognition*, Prentice Hall, NJ, USA, 1993.
[4] S. Esedoglu, "Blind deconvolution of bar code signals," *Inverse Problems*, vol. 20, no. 1, pp. 121–135, 2004.

[5] R. Acar and C. R. Vogel, "Analysis of bounded variation penalty methods for ill-posed problems," *Inverse Problems*, vol. 10, no. 6, pp. 1217–1229, 1994.

[6] T. F. Chan and C. K. Wong, "Total variation blind deconvolution," *IEEE Transactions on Image Processing*, vol. 7, no. 3, pp. 370–375, 1998.

[7] L. I. Rudin, S. Osher, and E. Fatemi, "Nonlinear total variation based noise removal algorithms," *Physica Ds*, vol. 60, no. 1-4, pp. 259–268, 1992.

[8] C. R. Vogel and M. E. Oman, "Fast, robust total variation-based reconstruction of noisy, blurred images," *IEEE Transactions on Image Processing*, vol. 7, no. 6, pp. 813–824, 1998.

[9] D. C. Dobson and F. Santosa, "Recovery of blocky images from noisy and blurred data," *SIAM Journal on Applied Mathematics*, vol. 56, no. 4, pp. 1181–1198, 1996.

[10] S. Osher and L. I. Rudin, "Feature-oriented image enhancement using shock filters," *SIAM Journal on Numerical Analysis*, vol. 27, no. 4, pp. 919–940, 1990.

[11] J. A. Sethian, *Level Set Methods*, vol. 3 of *Cambridge Monographs on Applied and Computational Mathematics*, Cambridge University Press, Cambridge, UK, 1996.

[12] P. Perona and J. Malik, "Scale-space and edge detection using anisotropic diffusion," *IEEE Transactions on Pattern Analysis and Machine Intelligence*, vol. 12, no. 7, pp. 629–639, 1990.

[13] S. Mallat and W. L. Hwang, "Singularity detection and processing with wavelets," *Institute of Electrical and Electronics Engineers. Transactions on Information Theory*, vol. 38, no. 2, part 2, pp. 617–643, 1992.

[14] A. Grossmann, "Wavelet transforms and edge detection," in *Stochastic Processes in Physics and Engineering*, M. Hazawinkel, Ed., vol. 42, pp. 149–157, Reidel, Dordrecht, The Netherlands, 1988.

[15] Y. Lu and R. C. Jain, "Reasoning about edges in scale space," *IEEE Transactions on Pattern Analysis and Machine Intelligence*, vol. 14, no. 4, pp. 450–468, 1992.

[16] J. Sun, D. Gu, Y. Chen, and S. Zhang, "A multiscale edge detection algorithm based on wavelet domain vector hidden Markov tree model," *Pattern Recognition*, vol. 37, no. 7, pp. 1315–1324, 2004.

[17] L. Zhang and P. Bao, "Edge detection by scale multiplication in wavelet domain," *Pattern Recognition Letters*, vol. 23, no. 14, pp. 1771–1784, 2002.

[18] S. Mallat, *A Wavelet Tour of Signal Processing*, Academic Press, San Diego, Calif, USA, 1998.

[19] J. Canny, "A computational approach to edge detection," *IEEE Transactions on Pattern Analysis and Machine Intelligence*, vol. 8, no. 6, pp. 679–698, 1986.

[20] E. Joseph and T. Pavlidis, "Bar code waveform recognition using peak locations," *IEEE Transactions on Pattern Analysis and Machine Intelligence*, vol. 16, no. 6, pp. 630–640, 1994.

[21] A. M. Vasilyev, *An Introduction To Statistical Physics*, Mir Publishers, Moscow, Russia, 1983.

[22] F. Reif, *Fundamentals of Statistical and Thermal Physics*, McGraw-Hill, New York, NY, USA, 1965.

[23] J. B. Johnson, "Thermal agitation of electricity in conductors," *Physical Review*, vol. 32, no. 1, pp. 97–109, 1928.

[24] H. Nyquist, "Thermal agitation of electric charge in conductors," *Physical Review*, vol. 32, no. 1, pp. 110–113, 1928.

[25] W. Schottky, "Über spontane Stromschwankungen in verschiedenen Elektrizitätsleitern," *Annalen der Physik*, vol. 362, no. 23, pp. 541–567, 1918.

[26] R. Sarpeshkar, T. Delbruck, and C. A. Mead, "White noise in MOS transistors and resistors," *IEEE Circuits and Devices Magazine*, vol. 9, no. 6, pp. 23–29, 1993.

[27] Y. M. Blanter and M. Büttiker, "Shot noise in mesoscopic conductors," *Physics Report*, vol. 336, no. 1-2, pp. 1–166, 2000.

[28] J. W. Goodman, "Statistical properties of laser speckle patterns," in *Laser Speckle and Related Phenomena*, J. C. Dainty, Ed., pp. 9–75, Springer, Berlin, Germany, 2nd edition, 1984.

[29] J. C. Dainty, "Recent Developments," in *Laser Speckle and Related Phenomena* , J. C. Dainty, Ed., pp. 321–337, Springer, Berlin, Germany, 2nd edition, 1984.

[30] T. Okamoto and T. Asakura, "The statistics of dynamic speckles," in *Progress in Optics*, E. Wolf, Ed., vol. 39, pp. 185–248, Elsevier Science, Amsterdam, The Netherlands, 1995.

[31] J. W. Goodman, *Introduction to Fourier Optics*, McGraw-Hill, New York, NY, USA, 2nd edition, 1996.

[32] E. Marom, S. Krešic-Jurić, and L. Bergstein, "Analysis of speckle noise in bar-code scanning systems," *Journal of the Optical Society of America A*, vol. 18, no. 4, pp. 888–901, 2001.

[33] D. Yu, M. Stern, and J. Katz, "Speckle noise in laser bar-code scanner systems," *Applied Optics*, no. 19, pp. 3687–3694, 1996.

[34] J. W. Goodman, *Statistical Optics*, Wiley, New York, NY, USA, 1985.

[35] G. R. Grimmett and D. R. Stirzaker, *Probability and Random Processes*, The Clarendon Press Oxford University Press, New York, NY, USA, 2nd edition, 1992.

[36] G. Gilbert, A. Aspect, and C. Fabre, *Introduction to Quantum Optics: from the Semi-Classical Approach to Quantized Light*, Cambridge University Press, Cambridge, UK, 2010.

[37] A. E. Ennos, "Speckle interferometry," in *Laser Speckle and Related Phenomena*, J. C. Dainty, Ed., pp. 203–253, Springer, Berlin, Germany, 2nd edition, 1984.

[38] J. Kim and H. Lee, "Joint nonuniform illumination estimation and deblurring for bar code signals," *Optics Express*, vol. 15, no. 22, pp. 14817–14837, 2007.

[39] D. Marr and E. Hildreth, "Theory of edge detection," *Proceedings of the Royal Society of London*, vol. 207, no. 1167, pp. 187–217, 1980.

[40] S. Krešić-Jurić, "Edge detection in bar code signals corrupted by integrated time-varying speckle," *Pattern Recognition*, vol. 38, no. 12, pp. 2483–2493, 2005.

[41] L. Wu and Z. Xie, "Scaling theorems for zero-crossings," *IEEE Transactions on Pattern Analysis and Machine Intelligence*, vol. 12, no. 1, pp. 46–54, 1990.